Dalton Transactions

2,2′-Disilylazobenzenes Featuring Double Intramolecular Nitrogen···Silicon Coordination: A Photoisomerizable Fluorophore

Journal:	*Dalton Transactions*
Manuscript ID:	DT-ART-05-2015-002038.R1
Article Type:	Paper
Date Submitted by the Author:	02-Jul-2015
Complete List of Authors:	Kano, Naokazu; The University of Tokyo, Department of Chemistry, Graduate School of Science Yamamura, Masaki; The University of Tokyo, Department of Chemistry, Graduate School of Science Kawashima, Takayuki; The University of Tokyo, Department of Chemistry, Graduate School of Science

Journal Name

ARTICLE

2,2′-Disilylazobenzenes Featuring Double Intramolecular Nitrogen···Silicon Coordination: A Photoisomerizable Fluorophore†

Received 00th January 20xx,
Accepted 00th January 20xx

DOI: 10.1039/x0xx00000x

www.rsc.org/

Naokazu Kano,*[a] Masaki Yamamura[a] and Takayuki Kawashima‡*[a]

(*E*)-4,4′-Dimethyl-2,2′-disilylazobenzenes were synthesized. Double intramolecular N···Si coordination in the bis(fluorodimethylsilyl) and bis(trifluorosilyl) derivatives was confirmed using X-ray crystallographic analysis and ^{29}Si NMR spectroscopy. In the absorption bands due to the π,π* transitions, introduction of silyl groups was found to cause a bathocromic shift. In contrast to most azobenzenes, which do not fluoresce at all, the (*E*)-2,2′-bis(trifluorosilyl)azobenzene derivative with the N···Si coordination fluoresced a yellow-green colour at room temperature. Methyl and trifluorosilyl groups lowered the n and π* orbitals, as revealed by the DFT calculations. As a result, the lowest singlet excitation energy state is found to be the allowed π,π* transition, different from the forbidden n,π* transition in general azobenzenes, by the TD-DFT calculations. The allowed transition character of the lowest singlet excited state and moderately rigid conformation of the azo moiety, provided by the double N···Si coordination, account for the fluorescence emission. Nevertheless, the N···Si coordination is weak enough to be cleaved upon photoexcitation, and thus the (*E*)-2,2′-disilylazobenzenes undergo photoisomerization to the (*Z*)-isomers. Both the photoisomerization and fluorescence emission properties of the azobenzene moiety have been achieved for the first time. After photoisomerization of the (*E*)-2,2′-disilylazobenzenes to the corresponding (*Z*)-isomer, they do not fluoresce. This change in the fluorescence intensity upon photoisomerization is useful for the regulation of fluorescence properties. Therefore, this compound can be recognized as a unique photoisomerizable fluorophore to regulate the fluorescence intensity using a single light source.

Introduction

Azobenzene, which is the fundamental core of azo dyes, is popular because of its reversible isomerization between the (*E*)- and (*Z*)-isomers upon photoirradiation. The photoisomerization property of azobenzene has been applied to molecular switches, photoregulation of biomaterials, light-driven molecular machines and molecular logic gates.[1] Its photoisomerization mechanism has been a subject of interest in photochemistry.[2] The photoisomerization property of azobenzene impedes its fluorescence emission, which is another property of some dyes.[3] Azobenzene derivatives are usually non-fluorescent or virtually non-fluorescent. Only a few azobenzene derivatives fluoresce as a fluorophore as a result of freezing in a matrix at low temperature,[4] ortho-metalation,[5] liquid crystal formation[6] or self-assembled aggregation.[7] In addition, whereas there are several photochromic switches for modulation of fluorescence emission,[8] there are only a few examples of azobenzene derivatives that undergo both photoisomerization and measurable fluorescence emission from their azobenzene moiety.[9] Such a photoisomerizable fluorophore is interesting for the purpose of regulation of fluorescence intensity by a single light source.[10]

We previously achieved intense fluorescence emission from (*E*)-2-borylazobenzenes (*E*)-**1** containing an electron-withdrawing bis(pentafluorophenyl)boryl group near the azo group (Chart 1).[11] A key for the fluorescent emission was the existence of an intramolecular nitrogen–boron interaction that could change the order of the singlet excited state by lowering the energy level of the n orbital of the azo group and locking the conformation to inhibit the isomerization. In (*E*)-2,2′-diborylazobenzenes (*E*)-**2**, the twofold intramolecular N–B interactions greatly lowered the energy level of the n orbital, facilitating its single-electron reduction.[12] The strong N–B interactions, however, suppressed photoisomerization, which is the most popular property of azobenzene, in both (*E*)-**1** and (*E*)-**2**. Thus, the fluorescent emission property was found to be gained at the cost of the photoisomerization property.

[a] *Department of Chemistry, Graduate School of Science, The University of Tokyo, 7-3-1 Hongo, Bunkyo-ku, Tokyo 113-0033, Japan. E-mail: kano@chem.s.u-tokyo.ac.jp*

† Electronic Supplementary Information (ESI) available: NMR spectral charts of (*E*)-**4a–e** and (*Z*)-**4a,d,e**, UV-vis spectra of (*E*)- and (*Z*)-**4a–e**, fluorescence spectra of (*E*)- and (*Z*)-**4e**, and TD-DFT calculations of (*E*)-**4e**, (*E*)-**5**, and (*E*)-**6**. See DOI: 10.1039/x0xx00000x

‡ Present address: Graduate School of Science and Technology, Gunma University, Gunma 376-8515, Japan. E-mail: kawashima.t@gunma-u.ac.jp

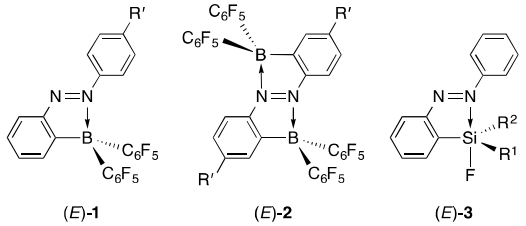

Chart 1

In our previous reports, we have found that several (*E*)-2-silylazobenzenes (*E*)-**3**, which bear an intramolecular nitrogen···silicon interaction, do not fluoresce.[13] Compounds (*E*)-**3** undergo photoisomerization accompanied by dissociation of the interaction in moderate to almost quantitative yields, indicating the weakness of the nitrogen···silicon interaction compared with the nitrogen–boron interaction. (*E*)-2,2′-Disilylazobenzenes featuring twofold weak nitrogen···silicon interactions are promising candidates for an isomerizable fluorophore because a few π-conjugated compounds containing the nitrogen···silicon interaction were recently reported to fluoresce.[14] Here, we report the synthesis and structures in both the crystalline and solution states of (*E*)-2,2′-disilylazobenzenes featuring intramolecular nitrogen···silicon interactions, together with their photophysical properties including photoisomerization and fluorescence emission. Their optical properties are discussed based on their spectroscopic measurements and DFT calculations.

Results and discussion

Synthesis

(*E*)-4,4′-Dimethyl-2,2′-disilylazobenzenes (*E*)-**4a–c** (Chart 2) were synthesized from (*E*)-2,2′-diiodo-4,4′-dimethylazobenzene and the corresponding chlorosilanes via the dilithiated (*E*)-4,4′-dimethylazobenzene according to the synthetic procedure for (*E*)-2,2′-bis(diphenylsilyl)-4,4′-dimethylazobenzene.[15] Methyl groups at the *para*-positions are necessary for their good solubility. Fluorination of (*E*)-**4b** with AgF gave (*E*)-**4d** bearing one fluorine atom on each silicon atom. Compound (*E*)-**4e** was synthesized by fluorination of (*E*)-**4c** with BF_3•OEt_2. Compounds (*E*)-**4a–e** can be handled in the air in the solid state, but (*E*)-**4d,e** are moisture sensitive and undergo hydrolysis easily in the solution state.

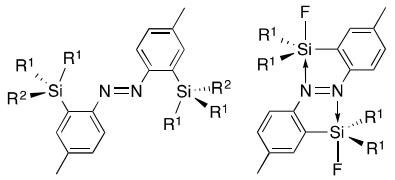

Chart 2

Crystal structure

The structures of (*E*)-4,4′-dimethyl-2,2′-disilylazobenzenes (*E*)-**4a,d,e** were determined using single-crystal X-ray crystallography to reveal the effects of the two silyl groups on the azobenzene structure.[16] Their thermal ellipsoid plots are shown in Figure 1. Selected bond lengths, bond angles and torsion angles are summarized in Table 1. All of the crystals show an almost planar structure of the azobenzene moiety. In (*E*)-**4a**, neither of the two silyl groups in a tetrahedral structure show an interaction with the azo moiety. This configuration is reasonable as a result of steric repulsion between the azo group and trimethylsilyl groups.

By contrast, both silyl groups in (*E*)-**4d,e** have the *syn* configuration with the N=N bond against the C1–N1 or C1*–N1* bond, as shown by the C2–C1–N1–N1* torsion angle, which is close to or equal to 0°. Nitrogen atoms occupy backside positions of a Si1–F1 bond with the N1*···Si1 interatomic distance (2.371(4)–2.585(3) Å) within the sum (3.65 Å) of the van der Waals radii of both elements.[17] The F1–Si1–C*n* and F1–Si1–F*n*′ bond angles are around 100° and narrower than the bond angle for a tetrahedral structure. These structural parameters show a capped tetrahedral coordination sphere at the silicon atoms as a result of a nitrogen···silicon dative bond on each silicon atom. In other words, each nitrogen atom of the azobenzene intramolecularly coordinates to a silicon atom, and its coordination reflects structural perturbation around the silicon atoms. Fluorine atoms increase the electrophilicity of the silicon atoms to a degree high enough to form the N···Si dative bonds, overcoming the steric repulsion between the silyl and azo groups. The N···Si interatomic distance in (*E*)-**4e** (2.367(4) Å) is shorter than that in (*E*)-**4d** (2.585(3) Å), reflecting the high electrophilicity of the silicon atom because of the introduction of more fluorine atoms. Such a tendency is also observed in (*E*)-2-silylazobenzenes (*E*)-**3**.[13] The N···Si interatomic distance in (*E*)-**4e** is slightly longer than that in (*E*)-**3a** (R^1 = R^2 = F; N···Si, 2.3030(14) Å),[13a] suggesting that the intramolecular coordination in (*E*)-2,2′-disilylazobenzenes is weaker than that in the corresponding (*E*)-2-monosilylazobenzenes and that the coordination is affected by other additional factors. Namely, in (*E*)-**4e**, attractive N1*···Si1 coordination should cause not only a shortening of the N1*···Si1 interatomic distance, but also narrowing and widening of C1–N1–N1* and N1–N1*–C1*, respectively, as in (*E*)-**3a**, in which the corresponding C–N–N and N–N–C angles are 111.7(1) and 119.9(1)°, respectively.[13] Because another coordination, N1···Si1* coordination, should cause opposite structural changes of the bond angles, the two conflicting N···Si interactions could not be too strong. Such a conflict makes the N···Si interatomic distance in (*E*)-**4e** slightly longer than that in (*E*)-**3**. The N···Si interactions in (*E*)-**4a,d,e** do not show significant changes in N=N bond distances (1.255(4)–1.274(4) Å).

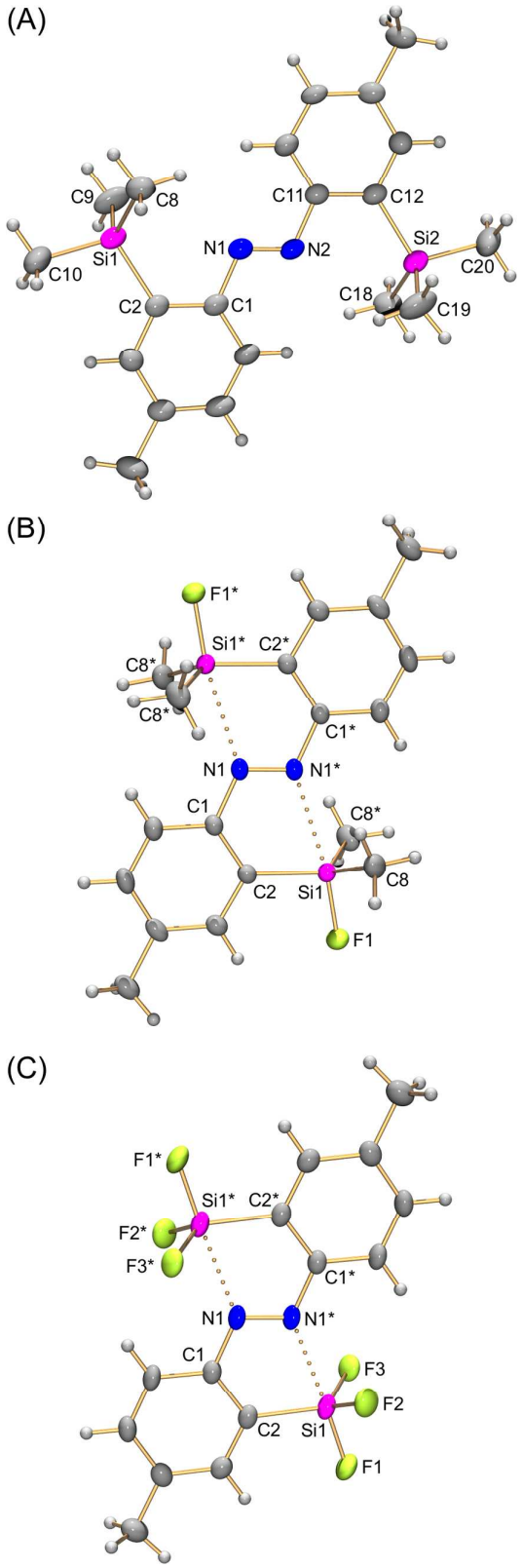

Figure 1. Thermal ellipsoid plots (50% probability) of (*E*)-2,2′-disilylazobenzenes (*E*)-**4a** (A), (*E*)-**4d** (B) and (*E*)-**4e** (C). Independent molecules of (*E*)-**4a** in the crystal unit cell are omitted.

Table 1. Selected bond lengths (Å), bond angles (°) and torsion angles (°) for (*E*)-2,2′-disilylazobenzenes (*E*)-**4a,d,e**.

		(*E*)-**4a**	
N1–N2	1.255(4)	C8–Si1–C10	107.4(2)
C2–Si1–C8	112.77(17)	C9–Si1–C10	108.6(2)
C2–Si1–C9	110.03(19)	C1–N1–N2	114.1(3)
C2–Si1–C10	107.18(18)	C2–C1–N1–N2	179.3(3)
C8–Si1–C9	110.6(2)		
		(*E*)-**4d**	
N1–N1*	1.274(4)	C2–Si1–C8	115.57(8)
N1*···Si1	2.585(3)	C8–Si1–C8*	119.09(14)
F1–Si1–C2	100.27(11)	C1–N1–N1*	113.4(3)
F1–Si1–C8	100.63(8)	C2–C1–N1–N1*	0.0(0)
		(*E*)-**4e**	
N1–N1*	1.255(6)	F2–Si1–F3	110.32(16)
N1*···Si1	2.371(4)	C2–Si1–F2	119.95(17)
F1–Si1–F2	99.93(16)	C2–Si1–F3	118.81(16)
F1–Si1–F3	101.11(16)	C1–N1–N1*	113.3(4)
F1–Si1–C2	102.18(17)	C2–C1–N1–N1*	0.6(5)

Structure in solution.

A weak N···Si coordination may dissociate in solution even if coordination exists in the crystalline state.[15] The ^{1}H, ^{13}C, ^{19}F and ^{29}Si NMR spectra of (*E*)-**4a–e** were measured for determination of their structures in solution. The magnitude of the contribution of the N···Si coordination in solution can be estimated by the ^{29}Si NMR chemical shifts, which reflect the coordination state of the silicon atoms. The ^{29}Si NMR chemical shifts of (*E*)-**4a–e** in $CDCl_3$ are summarized together with those of the corresponding silylbenzenes and differences ($\Delta\delta$) between their chemical shifts in Table 2. Compounds (*E*)-**4a–c** show chemical shifts that are almost the same as those of the corresponding silylbenzenes, with the difference being less than 1 ppm, indicating tetracoordination states of the silicon atoms. In contrast, compounds (*E*)-**4d,e** resonated upfield by 14–15 ppm. Such chemical shifts in (*E*)-**4d,e** indicate pentacoordination states of the silicon atoms also in solution. It is ascribed to the N···Si coordination, which is also found in the crystalline state.

Table 2. ^{29}Si NMR chemical shifts (ppm) of (*E*)-**4a–e** and the corresponding silylbenzenes, and their difference.

compound	SiR_3	δ((*E*)-**4**)	δ($PhSiR_3$)	$\Delta\delta^c$
(*E*)-**4a**	$SiMe_3$	–3.8	–4.1[a]	0.3
(*E*)-**4b**	$SiMe_2H$	–16.8	–17.6[b]	0.8
(*E*)-**4c**	$Si(OEt)_3$	–57.8	–57.8[a]	0.0
(*E*)-**4d**	$SiMe_2F$	4.9	19.8[b]	–14.9
(*E*)-**4e**	SiF_3	–87.7	–73.7[b]	–14.0

[a] Reference 18a. [b] Reference 18b. [c] $\Delta\delta = \delta$((*E*)-**4**) – δ($PhSiR_3$).

Photophysical properties

The photophysical properties of the (*E*)-4,4′-dimethyl-2,2′-disilylazobenzenes (*E*)-**4a–e** were studied using UV-vis absorption spectroscopy. The UV-vis absorption spectra of (*E*)-**4a–e** in hexane are shown in Figure 2. The absorption maxima of (*E*)-**4a–e** and (*E*)-4,4′-dimethylazobenzene ((*E*)-**5**) are summarized in Table 3. Compounds (*E*)-**4a–c** exhibited two absorption bands, a strong band in the short-wavelength region and a weak band in the long-wavelength region. The bands in the short- and long-wavelength regions are assigned to the allowed π,π* transition and the forbidden n,π* transition of the azobenzene moiety, respectively. Both of the bands are bathochromically shifted from the corresponding bands of non-silylated azobenzene (*E*)-**5**. The bathochromic shifts should be due to the inductive effect of the electron-donating silyl groups.[13,15]

In contrast, (*E*)-**4d,e** in the coordinating state exhibited a strong band with shoulder peaks and no other independent band. The band, ascribed to the π,π* transition, is much more bathochromically shifted than the bands of (*E*)-**4a–c**. The absorption maxima for the n,π* transition were not observed because their hypsochromic shifts would have caused their overlap with the strong π,π* absorption.[15]

Irradiation of a hexane solution of (*E*)-**4a–d** with UV light from a mercury lamp (λ = 365 nm) resulted in a decrease in the absorbance of the π,π* transition together with an increase of the absorbance of the n,π* transition (See, Electronic Supplementary Information). Subsequent irradiation of the reaction mixture with visible light (λ = 436 nm) recovered the strong π,π* absorbance of (*E*)-**4a–d**. These spectral changes correspond to reversible *E*,*Z*-photoisomerization of the azobenzene in (*E*)-**4a–d**. The *E*/*Z* ratio at the photostationary state of a $CDCl_3$ solution of (*E*)-**4a–d** under UV irradiation (λ = 365 nm) was determined to be 11/89, 2/98, 40/60, and 7/93, respectively, using ^{1}H NMR spectroscopy (see, Electronic Supplementary Information).

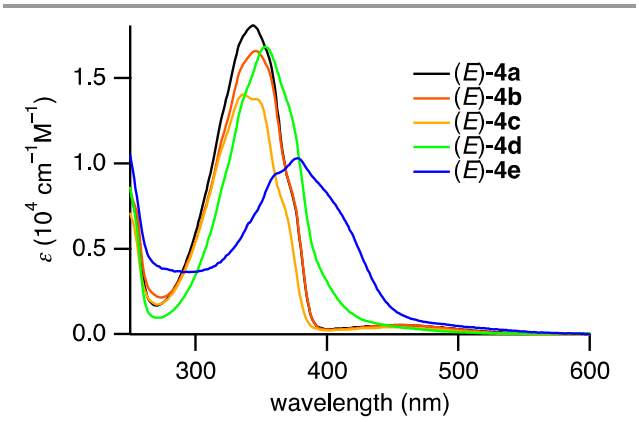

Figure 2. UV-vis absorption spectra of (*E*)-**4a–e** in hexane.

Table 3. Absorption maxima of (*E*)-**4a–e** and (*E*)-**5** in hexane.

	λ_{max}/nm (ε/cm^{-1} M^{-1})	
	π,π*	n,π*
(*E*)-**4a**	343 (18100)	457 (530)
(*E*)-**4b**	345 (16600)	457 (540)
(*E*)-**4c**	345 (13800)	452 (400)
(*E*)-**4d**	353 (16800)	–
(*E*)-**4e**	378 (10200)	–
(*E*)-**5**	330 (27000)[a,b]	444 (630)[a,b]

a. In cyclohexane. *b*. Reference 19.

Similar to (*E*)-**4a–d**, exposure of a hexane solution of (*E*)-**4e** to UV light (λ = 365 nm) resulted in a decrease in the absorbance of π,π* transition at 384 nm, which was recovered by irradiating the solution with visible light (λ = 436 nm). The UV-vis spectral changes with isosbestic points during the photoirradiation are shown in Figure 3. These spectral changes correspond to reversible *E*,*Z*-photoisomerization of azobenzene in (*E*)-**4e**. The *E*/*Z* ratio at the photostationary state under UV irradiation (λ = 365 nm) of a hexane solution was determined to be 79:21 using ^{19}F NMR spectroscopy (see, Electronic Supplementary Information).

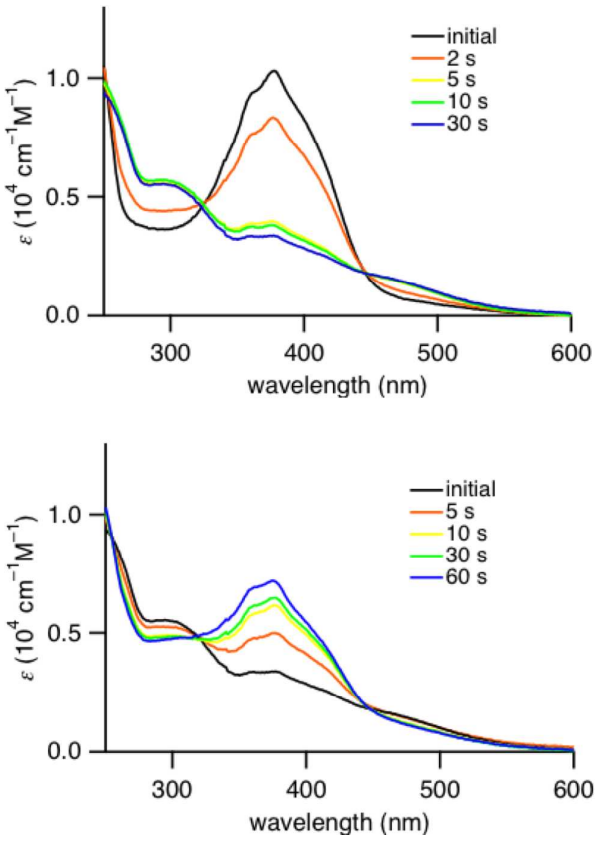

Figure 3. Change of UV-vis absorption spectra of (*E*)-**4e** in hexane upon photoirradiation with a mercury lamp (λ = 365 nm) (above) and upon photoirradiation (λ = 436 nm) (below).

Interestingly, (*E*)-**4e** in hexane exhibited yellow-green fluorescence at 568 nm at room temperature (Figure 4). The quantum yield for (*E*)-**4e** was determined to be 0.060 in chloroform by an integrating sphere method. Its quantum yield in hexane was similarly determined to be 0.024. These values are significantly larger than the 2.53×10^{-5} for the unsubstituted azobenzene (PhN=NPh).[20] Although the fluorescence quantum yield is much smaller than the 0.73 for (*E*)-2,2′-diborylazobenzene (*E*)-**2** (R′ = Bu),[12] fluorescence emission of (*E*)-**4e** is worth mentioning because most azobenzene derivatives, including (*E*)-2-silylazobenzenes, (*E*)-**3**, do not fluoresce at all. Considering the photophysical properties, (*E*)-2,2′-disilylazobenzene (*E*)-**4e** was found to be an azobenzene derivative that gives rise to photoisomerization in the excited state and fluorescence from the azo moiety at room temperature.

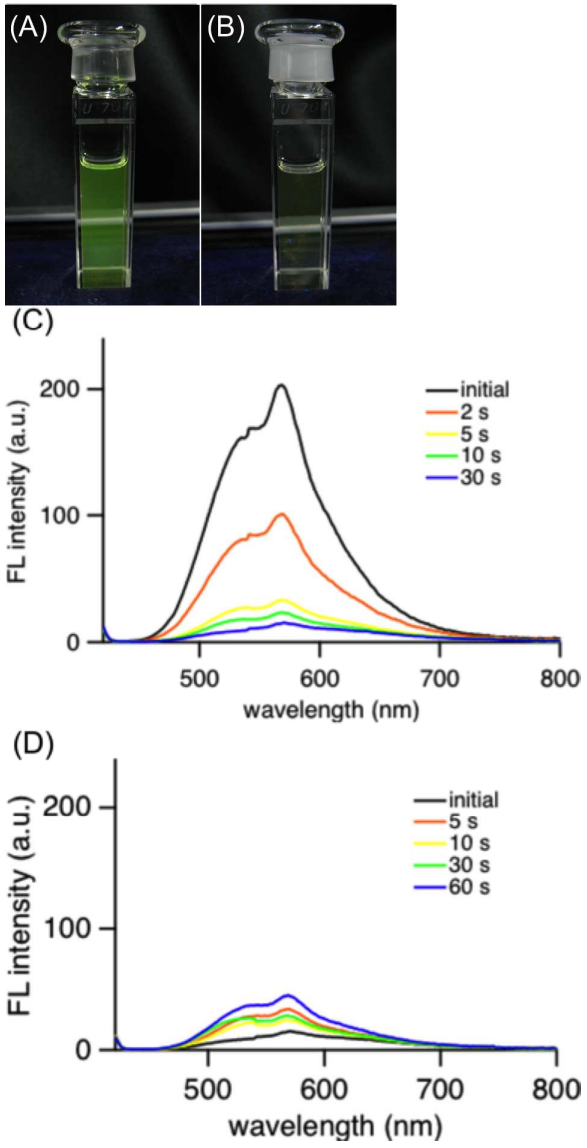

Figure 4. Photograph of (*E*)-**4e** in hexane under photoirradiation in the dark (mercury lamp, 400 W, λ = 365 nm) (A) and after irradiation for a minute (B), change of fluorescence spectra (λ_{ex} = 380 nm) of (*E*)-**4e** in hexane upon photoirradiation (λ = 365 nm) (C) and change of fluorescence spectra upon photoirradiation (λ = 436 nm) (D).

Upon photoirradiation, as the fraction of the (*E*)-isomer of **4e** in a mixture of (*E*)- and (*Z*)-isomers of **4e** decreased, the fluorescence intensity weakened (Figure 4(C)). Finally, at the photostationary state, the mixture fluoresced very weakly, to the extent of almost non-fluorescence. The fluorescent yellow-green colour of the solution changed to non-fluorescent pale yellow (Figure 4(A),(B)). This result can be explained by supposing that (*Z*)-**4e** formed from fluorescent (*E*)-**4e** does not fluoresce at all. The photoisomerization decreased the fraction of (*E*)-**4e** so that the fluorescence intensity should also decrease in proportion to the fraction of (*E*)-**4e**. After a mixture of (*E*)- and (*Z*)-**4e** had reached the photostationary state with light of λ = 365 nm, the solution was irradiated with light of λ = 436 nm and the fluorescence intensity increased in a reflection of the (*E*)/(*Z*) ratio at another photostationary state upon irradiation (Figure 4(D)).

Structure of (Z)-2,2′-disilylazobenzene

The photophysical property of the (*Z*)-isomer is considered to be related to its structure. Taking into account the high *E*,*Z*-photoisomerization efficiency, which facilitates both the characterization and isolation of the (*Z*)-isomer, the structure of (*Z*)-**4d** was studied using ^{29}Si NMR spectroscopy and single-crystal X-ray crystallography. The ^{29}Si NMR spectrum of (*Z*)-**4d** in $CDCl_3$ showed a doublet at a chemical shift of 22.2 ppm with a coupling constant of 274 Hz. The chemical shift, which is close to that (δ 19.8 ppm) of fluorodimethylsilylbenzene, suggests the absence of the N···Si coordination of (*Z*)-**4d**, similar to (*Z*)-**3**. Recrystallization of (*Z*)-**4d** in the dark gave single crystals, which were used for the single-crystal X-ray crystallography. The crystal structure of (*Z*)-**4d** depicted in Figure 5 clearly shows the (*Z*)-conformation of azobenzene and the lack of N···Si coordination. The N1–N2 bond length (1.256(2) Å) is reasonable for an azobenzene. Thus, it is reasonable that fluorescence was suppressed severely in the mixture containing a certain amount of the (*Z*)-isomer after the photoisomerization, if the presence of the N···Si interaction is a key for the fluorescence emission.

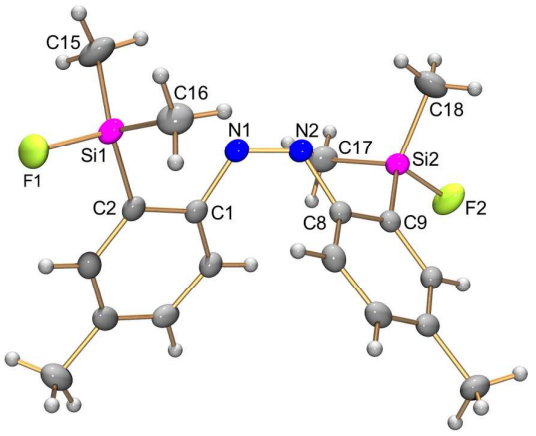

Figure 5. Thermal ellipsoid plot (50% probability) of (*Z*)-2,2′-disilylazobenzene (*Z*)-**4d**. Selected bond lengths (Å), angles (°) and torsion angles (°): N1–N2, 1.256(2); Si1–F1, 1.611(1); Si2–F2, 1.610(1); C1–N1–N2, 123.5(1); N1–N2–C8, 122.5(1); F1–Si1–C2, 103.57(6); F1–Si1–C15, 106.21(8); F1–Si1–C16, 106.50(8); C1–N1–N2–C8, –8.7(2).

Theoretical calculations

Theoretical calculations were performed to shed light on the effects of the N···Si coordination on the optical properties of (*E*)-**4e**. The structures of (*E*)-4,4′-dimethyl-2,2′-disilylazobenzene (*E*)-**4e**, non-silylated (*E*)-4,4′-dimethylazobenzene ((*E*)-**5**) and (*E*)-4,4′-dimethyl-2-(trifluorosilyl)azobenzene ((*E*)-**6**) were optimized using density functional theory (DFT) calculations at the B3PW91/6-31G(d,p) level. The optimized structures of (*E*)-**4e** and (*E*)-**5**, whose structures were confirmed by single-crystal X-ray crystallography,[21] reproduced the corresponding crystal structures very well. For example, the N–N bond lengths and N···Si interatomic distances of the optimized structures ((*E*)-**4e**, N–N, 1.255 Å, N···Si, 2.369 Å; (*E*)-**5**, N–N, 1.259 Å) matched well with the corresponding values in the crystal structures ((*E*)-**4e**, N–N, 1.255(6) Å, N···Si, 2.371(4) Å; (*E*)-**5**, N–N, 1.263(2) Å). Energy diagrams of the Kohn-Sham orbitals of (*E*)-**4e**, (*E*)-**5** and (*E*)-**6** were obtained at the B3PW91/6-311++G(2d,p) level (Figure 6). The HOMO and LUMO of (*E*)-**4e**, (*E*)-**5** and (*E*)-**6** are composed of π and π* orbitals, respectively, spreading over the azobenzene moiety. The HOMO–1 of (*E*)-**5** and (*E*)-**6** is composed of the n orbital. Thus, the HOMO character of all three compounds is different from that of non-substituted (*E*)-azobenzene ((*E*)-Ph–N=N–Ph), in which the HOMO is mainly composed of the n orbital. To discuss substituent effects on the molecular orbitals and their energy levels, both methyl and trifluorosilyl groups should be considered. In (*E*)-**5**, the energy gap between the π orbital, HOMO (energy level *E*, –6.20 eV), and the n orbital, HOMO–1 (*E*, –6.36 eV), is very small (Δ*E*, 0.16 eV), even though the order has been inverted compared with that in non-substituted azobenzene.

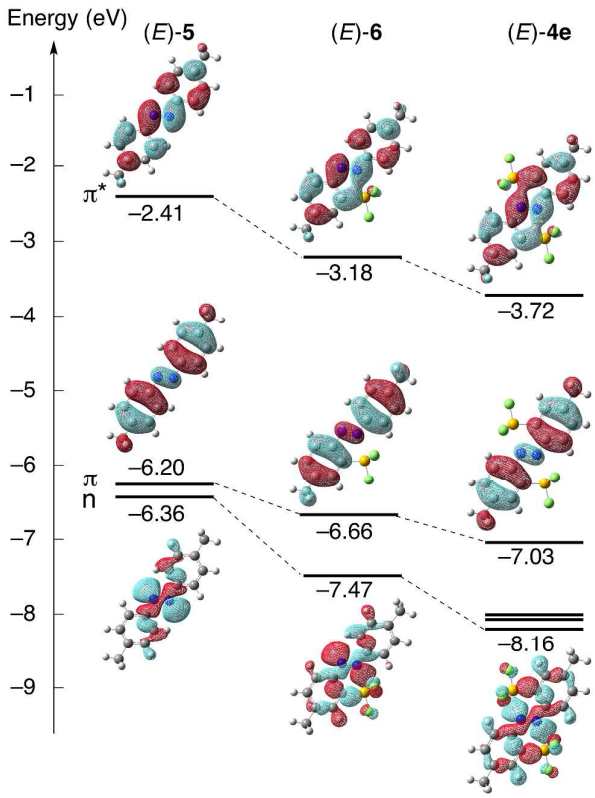

Figure 6. Energy diagrams of the Kohn–Sham frontier orbitals of (*E*)-**4e** (right), (*E*)-**5** (left) and (*E*)-**6** (middle) at the B3PW91/6-31G(d,p)//B3PW91/6-311++G(2d,p) level: white, hydrogen; grey, carbon; blue, nitrogen; yellow-green, fluorine; orange, silicon.

In both (*E*)-**6** and (*E*)-**4e** bearing trifluorosilyl groups, the n orbitals are used for the coordination to silicon atoms, and the N···Si coordination causes a large stabilization of the orbitals. As a result, the gap between the n orbital and the HOMO, π orbital, becomes large in both (*E*)-**4e** and (*E*)-**6** ((*E*)-**4e**, Δ*E*, 1.13 eV; (*E*)-**6**, Δ*E*, 0.81 eV). In addition, it is noteworthy that the p-orbital of the silicon is involved in the LUMO in (*E*)-**4e** and (*E*)-**6**. This orbital overlap is assigned to σ*–π* conjugation, which is common in some π-conjugated compounds, such as a silole bearing heavier elements.[22] The N···Si coordination leads to σ*–π* conjugation and a decrease in the LUMO energy level. The LUMO energy level decreases in the order (*E*)-**5**, (*E*)-**6** and (*E*)-**4e**, reflecting the magnitude of the σ*–π* conjugation. The σ*–π* conjugation in the LUMO accounts for the large energy gaps between the LUMO of (*E*)-**5** and LUMOs of (*E*)-**6** and (*E*)-**4e**. Relatively small energy gaps between the HOMO of (*E*)-**5** and HOMOs of (*E*)-**6** and (*E*)-**4e** are reasonable because the conjugation is not involved in the HOMO while it is more dominant in the LUMO.

Vertical excitation energies were obtained using time-dependent DFT (TD-DFT) calculations at the B3PW91/6-311++G(2d,p) level based on the optimized structures. Diagrams of the excitation energies of (*E*)-**4e**, (*E*)-**5** and (*E*)-**6** are shown in Figure 7. The transition from the ground state, S_0, to the lowest singlet excited state, S_1, for (*E*)-**5**, which has no silyl group, corresponds to the transition from HOMO–1 to LUMO, and it is assignable to the forbidden n,π* transition (excitation energy *E*, 2.60 eV; oscillator strength *f*, 0.0000) (see, Electronic Supplementary Information). The character of the $S_0 \rightarrow S_1$ transition is the same as that of non-substituted (*E*)-azobenzene, in which the $S_0 \rightarrow S_1$ transition corresponds to the n,π* transition. The transition between S_0 and the second singlet excited state, S_2, for (*E*)-**5** corresponds to the transition from HOMO to LUMO, and it is assignable to the π,π* transition (*E*, 3.54 eV; *f*, 0.9510). In contrast, the $S_0 \rightarrow S_1$ transition for (*E*)-**4e** corresponds to the HOMO → LUMO transition, which is assignable to the allowed π,π* transition (*E*, 3.02 eV; *f*, 0.6421), and the $S_0 \rightarrow S_2$ transition corresponds to the HOMO–3 → LUMO transition, which is assignable to the forbidden n,π* transition (*E*, 3.18 eV; *f*, 0.0000). In (*E*)-**4e**, the singlet excitation energy of the π,π* transition has decreased, reflecting the large stabilization of the π* orbital because of the σ*–π* conjugation. The singlet excitation energy of the n,π* transition has increased, reflecting the stabilization of the n orbital. As a result, the order of the n,π* and π,π* transitions for (*E*)-**4e** is inverted from that for (*E*)-**5**. These results of the calculations indicate that the coordination of the azo moiety to the silicon atoms greatly contributes to the perturbation of both the electronic structures and excitation energies.

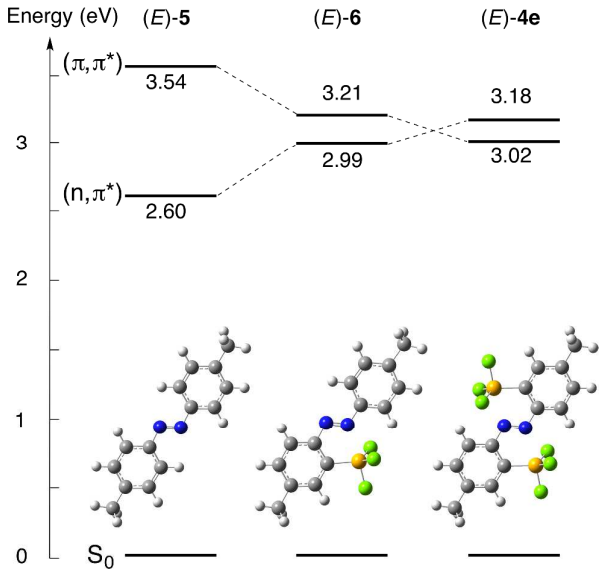

Figure 7. Energy diagrams of the singlet excitation energies of (*E*)-**4e** (right), (*E*)-**5** (left) and (*E*)-**6** (middle) at the B3PW91/6-31G(d,p)//B3PW91/6-311++G(2d,p) level together with their optimized structures.

The singlet excitation energy of the π,π* transition (*E*, 3.21 eV; *f*, 0.7416) for (*E*)-4,4′-dimethyl-2-silylazobenzene (*E*)-**6** has decreased significantly from that of (*E*)-**5**, but it remains above the increased energy level of the n,π* transition (*E*, 2.99 eV; *f*, 0.0009). The single N···Si coordination in (*E*)-**6** is found to be too weak to invert the order of the energy levels from that in (*E*)-**5**. Therefore, the double coordination to the two silicon atoms in (*E*)-**4e** is crucial for the inversion of the order of n,π* and π,π* transitions. The allowed π,π* transition energies decrease in the order (*E*)-**5**, (*E*)-**6** and (*E*)-**4e**. The π,π* transition energy of (*E*)-**4e** being lower than that of (*E*)-**5** is consistent with the bathochromic shift of the corresponding absorption bands in the UV-vis absorption spectrum of (*E*)-**4e**.

The results of the theoretical calculations explain why (*E*)-**4e** fluoresces. Before giving the explanation, we would like to describe a reason why popular azobenzene derivatives cannot fluoresce. Most (*E*)-azobenzene derivatives, such as (*E*)-**5**, are excited by photoirradiation and slowly relax to the S_1 state by internal conversion. They cannot fluoresce because the $S_1 \rightarrow S_0$ transition is the forbidden n,π* transition. Instead, the photoexcitation energy is used for isomerization to the corresponding (*Z*)-isomer or a non-radiative relaxation such as molecular vibration. By contrast, in (*E*)-**4e**, the $S_1 \rightarrow S_0$ transition is not a forbidden n,π* transition, but an allowed π,π* transition owing to the double N···Si coordination. Furthermore, the rigid structure because of the interaction prohibits non-radiative relaxation to some extent. Thus, upon photoirradiation, excited (*E*)-**4e** can relax from S_1 to S_0 accompanied by fluorescence emission. This is a reason for the fluorescence emission of (*E*)-**4e**.

Although the fluorescence emission of (*E*)-**4e** is explained similarly to that of (*E*)-**1** and (*E*)-**2** featuring N···B coordination,[11,12] we need an answer for the question why (*E*)-**4e** photoisomerizes as well as fluoresces. A reason for the photoisomerization property of (*E*)-**4e** is the weaker N···Si coordination than that in (*E*)-2-trifluorosilylazobenzene, as revealed by the X-ray crystallographic analysis. The weak N···Si coordination should be cleaved during/after the photoexcitation, and isomerization should occur during the non-radiative decay process. Considering that (*E*)-2-trifluorosilylazobenzene, which has stronger N···Si coordination than (*E*)-**4e**, can isomerize upon photoirradiation,[13d] it is reasonable that (*E*)-**4e** can undergo photoisomerization by competing with the fluorescence emission process. The weak N···Si coordination of (*E*)-**4e** should be a key for the bifunctional character, fluorescence emission and photoisomerization, the latter of which cannot be achieved in the fluorescent (*E*)-2-diborylazobenzenes (*E*)-**1** and (*E*)-2,2′-diborylazobenzenes (*E*)-**2**.

Experimental

General procedure

THF and diethyl ether (Et_2O) were distilled from sodium and benzophenone before use. All reactions were carried out in oven-dried glassware under argon atmosphere. 2,2′-Diiodo-4,4′-dimethylazobenzene was synthesized according to literature. The ^{1}H NMR (600, 500 and 400 MHz), ^{13}C NMR (150, 126 and 100 MHz) and ^{29}Si NMR (99 MHz) spectra were recorded on a JEOL A500 and AL400 or Bruker AVANCE600 spectrometers using tetramethylsilane (TMS) as an internal standard. The ^{19}F NMR (376 MHz) spectra were recorded on a JEOL AL400 spectrometer using Freon as an external standard. All melting points are uncorrected. Elemental analyses were performed by the Microanalytical Laboratory of Department of Chemistry, Faculty of Science, The University of Tokyo.

Synthesis of (E)-2,2′-disilylazobenzenes

Compounds (*E*)-**2a-c** were synthesized from (*E*)-2,2′-diiodo-4,4′-dimethylazobenzene according to the procedure reported previously in the reference.[15]

(*E*)-4,4′-Dimethyl-2,2′-bis(trimethylsilyl)azobenzene ((*E*)-4a): orange crystals; yield 99%; m.p. 173-174 °C; ^{1}H NMR (600 MHz, $CDCl_3$) δ 0.37 (s, 18H), 2.43 (s, 6H), 7.28 (dd, ^3J = 8.4 Hz, ^4J = 1.3 Hz, 2H), 7.47 (d, ^4J = 1.3 Hz, 2H), 7.63 (d, ^3J = 8.3 Hz, 2H); ^{13}C{^{1}H} NMR (100 MHz, $CDCl_3$) δ 0.59, 21.52, 114.46, 130.75, 135.30, 139.86, 142.54, 155.39; ^{29}Si NMR (99 MHz, $CDCl_3$) δ −3.76 (s); UV/vis (hexane) λ_{max} (ε) 343 (1.81×10^4), 457 nm (5.3×10^2); Anal. Calcd for $C_{20}H_{30}N_2Si_2$: C, 67.74; H, 8.53; N, 7.90. Found: C, 67.57%; H, 8.59; N, 7.85%.

(*E*)-2,2′-Bis(dimethylsilyl)-4,4′-dimethylazobenzene ((*E*)-4b): orange crystals; yield 74%; m.p. 117-118 °C; ^{1}H NMR (600 MHz, $CDCl_3$) δ 0.43 (d, ^3J = 3.5 Hz, 12H), 2.43 (s, 6H), 4.66 (sept, ^3J = 3.5 Hz, $^1J_{Si-H}$ = 190.2 Hz, 2H), 7.30 (dd, ^3J = 8.4 Hz, ^4J = 1.4 Hz, 2H), 7.54 (d, ^4J = 1.4 Hz, 2H), 7.66 (d, ^3J = 8.4 Hz, 2H); ^{13}C{^{1}H} NMR (100 MHz, $CDCl_3$) δ −2.18, 21.47, 114.79, 131.20, 136.28, 140.30, 140.34, 155.23; ^{29}Si NMR (99 MHz, $CDCl_3$) δ −16.79 (dsept, $^1J_{Si-H}$ = 190.2 Hz, $^2J_{Si-H}$ = 6.6 Hz); UV/vis (hexane) λ_{max} (ε)

345 (1.66×10^4), 457 nm (5.4×10^2); Anal. Calcd for $C_{18}H_{26}N_2Si_2$: C, 66.20; H, 8.02; N, 8.58. Found: C, 65.99; H, 8.09; N, 8.36%.

(*E*)-4,4′-Dimethyl-2,2′-bis(triethoxysilyl)azobenzene ((*E*)-4c): orange crystals; yield 37%; m.p. 115-116 °C; ^{1}H NMR (600 MHz, $CDCl_3$) δ 1.18 (t, ^3J = 7.2 Hz, 18H), 2.44 (s, 6H), 3.86 (q, ^3J = 7.2 Hz, 12H), 7.34 (dd, ^3J = 8.4 Hz, ^4J = 1.4 Hz, 2H), 7.79 (d, ^4J = 1.4 Hz, 2H), 7.89 (d, ^3J = 8.4 Hz, 2H); ^{13}C{^{1}H} NMR (100 MHz, $CDCl_3$) δ 18.14, 21.50, 58.60, 114.80, 132.20, 133.62, 137.67, 140.40, 155.59; ^{29}Si NMR (99 MHz, $CDCl_3$) δ −57.76 (s); UV/vis (hexane) λ_{max} (ε) 345 (1.38×10^4), 452 nm (4.0×10^2); Anal. Calcd for $C_{26}H_{42}N_2O_6Si_2$: C, 58.39; H, 7.92; N, 5.24. Found: C, 58.25; H, 7.80; N, 5.04%.

Synthesis of (*E*)-2,2′-bis(fluorodimethylsilyl)-4,4′-dimethylazobenzene ((*E*)-4d)

To a THF solution (20 mL) of **(*E*)-4b** (144 mg, 0.440 mmol) was added silver(I) fluoride (451.1 mg, 3.55 mmol) at ambient temperature and the reaction mixture was stirred for 20 hours. After the residual salt was filtered off, the filtrate was concentrated. The crude product was purified by preparative HPLC to give yellow crystals of **(*E*)-4d** (119 mg, 0.328 mmol, 75%).

(*E*)-4d: yellow crystals; yield 75%; m.p. 179-180 °C; ^{1}H NMR (600 MHz, $CDCl_3$) δ 0.48 (d, $^3J_{F-H}$ = 3.2 Hz, 12H), 2.48 (s, 6H), 7.44 (dd, ^3J = 8.4 Hz, ^4J = 1.4 Hz, 2H), 7.80 (d, ^4J = 1.4 Hz, 2H), 7.89 (d, ^3J = 8.4 Hz, 2H);^{13}C{^{1}H} NMR (100 MHz, $CDCl_3$) δ 1.36 (d, $^2J_{C-F}$ = 19.2 Hz), 21.62 (s), 125.17 (s), 131.66 (s), 131.73 (d, $^2J_{C-F}$ = 15.7 Hz), 136.71 (d, $^3J_{C-F}$ = 6.8 Hz), 142.11 (s), 152.44 (d, $^3J_{C-F}$ = 2.4 Hz); ^{19}F NMR (376 MHz, $CDCl_3$) δ −149.17 (brs, $^1J_{Si-F}$ = 265.6 Hz); ^{29}Si NMR (99 MHz, $CDCl_3$) δ 4.91 (d, $^1J_{Si-F}$ = 265.6 Hz); UV/vis (hexane) λ_{max} (ε) 353 nm (1.68×10^4); Anal. Calcd for $C_{18}H_{24}N_2F_2Si_2$: C, 59.63; H, 6.67; N, 7.73. Found: C, 59.84; H, 6.74; N, 7.53%.

Synthesis of (*E*)-4,4′-dimethyl-2,2′-bis(trifluorosilyl)azobenzene ((*E*)-4e)

To an ether solution (10 mL) of (*E*)-**4c** (54.5 mg, 0.102 mmol) was added boron trifluoride-diethyl ether (50 μL, 0.40 mmol) at ambient temperature and the reaction mixture was stirred for 6 hours. After the reaction mixture was concentrated, dry hexane was added. The insoluble product was filtered off and the filtrate was concentrated. The crude product was purified by recrystallization from hexane to give yellow crystals of **(*E*)-4e** (8.1 mg, 0.021 mmol, 21%). Compound **(*E*)-4e** was gradually decomposed.

(*E*)-4e; yellow crystals; ^{1}H NMR (600 MHz, C_6D_6) δ 1.80 (s, 6H), 6.83 (d, ^3J = 8.0 Hz, 2H), 7.64 (s, 2H), 8.07 (d, ^3J = 8.0 Hz, 2H); ^{13}C{^{1}H} NMR (150 MHz, C_6D_6) δ 20.80, 129.42, 134.67, 139.97, 145.10 (two aromatic carbons were not observed probably due to the complex coupling with fluorine atoms); ^{19}F NMR (376 MHz, $CDCl_3$) δ −140.72 (s, $^1J_{Si-F}$ = 237.4 Hz); ^{29}Si NMR (99 MHz, $CDCl_3$) δ −87.73 (q, $^1J_{Si-F}$ = 237.4 Hz); UV/vis (hexane) λ_{max} (ε) 378 nm (1.02×10^4).

Typical procedure for photoisomerization of 2,2′-disilylazobenzenes

A $CDCl_3$ solution of **(*E*)-4a** (5.8 mM, 0.5 mL) in a Pyrex NMR tube was irradiated with emission line at 365 nm from high-pressure mercury lamp (500 W) through a colored-glass filter for two hours at room temperature. In ^{1}H NMR spectrum, new signals assigned to **(*Z*)-4a** were observed. The ratio of **(*E*)-4a** and **(*Z*)-4a** was determined to be 13:87 by the integral of the NMR signals. Further irradiation at 365 nm did not change the ratio. The reaction mixture was irradiated with emission line at 436 nm for two hours at room temperature, and then the ratio of **(*E*)-4a** and **(*Z*)-4a** was changed to be 84:16. Further irradiation at 436 nm did not change the ratio.

(*Z*)-4a: red solution in $CDCl_3$; *E*/*Z*, 11/89 (at the photostationary state, λ = 365 nm), 84/16 (λ = 436 nm); ^{1}H NMR (600 MHz, $CDCl_3$) δ 0.40 (s, 18H), 2.28 (s, 6H), 5.90 (d, ^3J = 8.4 Hz, 2H), 6.78 (dd, ^3J = 8.4 Hz, ^4J = 1.4 Hz, 2H), 7.38 (d, ^4J = 1.4 Hz, 2H); ^{13}C{^{1}H} NMR (126 MHz, $CDCl_3$) δ −0.04, 21.26, 122.76, 129.01, 129.28, 135.98, 136.35, 156.57; ^{29}Si NMR (99 MHz, $CDCl_3$) δ −3.62 (s).

(*Z*)-4b: red solution in $CDCl_3$; *E*/*Z*, 12/88 (365 nm), 80/20 (436 nm); ^{1}H NMR (500 MHz, $CDCl_3$) δ 0.45 (d, ^3J = 3.5 Hz, 12H), 2.21 (s, 6H), 4.60 (sept, ^3J = 3.5 Hz, $^1J_{Si-H}$ = 191.5 Hz, 2H), 5.94 (d, ^3J = 8.4 Hz, 2H), 6.82 (dd, ^3J = 8.4 Hz, ^4J = 1.4 Hz, 2H), 7.43 (d, ^4J = 1.4 Hz, 2H).

(*Z*)-4c: red solution in $CDCl_3$; *E*/*Z*, 40/60 (365 nm), 80/20 (436 nm); ^{1}H NMR (600 MHz, $CDCl_3$) δ 1.26 (t, ^3J = 7.2 Hz, 18H), 2.26 (s, 6H), 4.00 (q, ^3J = 7.2 Hz, 12H), 6.19 (d, ^3J = 8.4 Hz, 2H), 6.84 (dd, ^3J = 8.4 Hz, ^4J = 1.4 Hz, 2H), 7.58 (d, ^4J = 1.4 Hz, 2H).

(*Z*)-4d: red solution in $CDCl_3$; *E*/*Z*, 7/93 (λ = 365 nm), 83/17 (λ = 436 nm); ^{1}H NMR (500 MHz, $CDCl_3$) δ 0.58 (d, $^3J_{F-H}$ = 7.8 Hz, 12H), 2.32 (s, 6H), 5.98 (d, ^3J = 8.4 Hz, 2H), 6.88 (dd, ^3J = 8.4 Hz, ^4J = 1.4 Hz, 2H), 7.56 (d, ^4J = 1.4 Hz, 2H); ^{13}C{^{1}H} NMR (126 MHz, $CDCl_3$) δ −0.05 (d, $^2J_{C-F}$ = 15.1 Hz), 21.13 (s), 114.91 (s), 130.57 (s), 133.90 (d, $^2J_{C-F}$ = 12.8 Hz), 135.17 (d, $^3J_{C-F}$ = 3.3 Hz), 137.14 (s), 155.87(s); ^{19}F{^{1}H} NMR (376 MHz, $CDCl_3$) δ −162.64 (s, $^1J_{Si-F}$ = 273.6 Hz); ^{29}Si NMR (99 MHz, $CDCl_3$) δ 22.19 (d, $^1J_{Si-F}$ = 273.6 Hz).

(*Z*)-4e: red solution in hexane; *E*/*Z*, 21/79 (λ = 365 nm), 40/60 (λ = 436 nm); ^{1}H NMR (500 MHz, $CDCl_3$) δ 2.37 (s, 6H), 6.17 (d, ^3J = 8.0 Hz, 2H), 7.10 (d, ^3J = 8.0 Hz, 2H), 7.74 (s, 2H); ^{19}F NMR (376 MHz, $CDCl_3$) δ −137.49 (s).

X-ray crystallographic analysis of (*E*)-4a,d,e

The X-ray diffraction data were collected on a CCD diffractometer with a graphite-monochromated Mo-Kα radiation. Diffraction data were processed using CrystalClear (Rigaku) for (*E*)-**4a,d** and Bruker SAINT (Bruker) for (*E*)-**4e**. The intensities were corrected for Lorentz and polarization effects. The structures were solved by direct methods (SHELXS-97) and expanded using Fourier techniques. Non-hydrogen atoms were refined anisotropically. Hydrogen atoms were put at calculated positions and refined isotropically. Crystallographic data of (*E*)-**4a**: $C_{20}H_{30}N_2Si_2$, MW = 354.64, triclinic, *P*–*1*, *a* = 10.132(5) Å, *b* = 13.834(9) Å, *c* = 16.460(11) Å, α = 91.96(2)°, β = 91.53(3)°, γ = 110.682(17)°, *V* = 2155(2) Å^3, *Z* = 4, μ(Mo-Kα) = 0.169 mm^{-1},

D_c = 1.093 g cm^{-3}, T = 120 K, 7330 measured and 5155 independent reflections, 449 parameters, R_1 ($I > 2\sigma(I)$) = 0.0769, wR_2 (all data) = 0.1651, GOF = 1.112. (*E*)-**4d**: $C_{18}H_{24}N_2F_2Si_2$, MW = 362.57, orthorhombic, *Cmca*, a = 7.290(5) Å, b = 16.889(12) Å, c = 15.688(12) Å, $\alpha = \beta = \gamma = 90°$, V = 1932(2) Å^3, Z = 4, μ(Mo-Kα) = 0.204 mm^{-1}, D_c = 1.247 g cm^{-3}, T = 130 K, 1176 measured and 973 independent reflections, 72 parameters, R_1 ($I > 2\sigma(I)$) = 0.0473, wR_2 (all data) = 0.1286, GOF = 1.117. (*Z*)-**4d**: $C_{18}H_{24}N_2F_2Si_2$, MW = 362.57, triclinic, *P*–1, a = 8.9666(5) Å, b = 10.7053(7) Å, c = 11.2276(7) Å, α = 93.383(2)°, β = 106.763(2)°, γ = 99.798(2)°, V = 1010.2(2) Å^3, Z = 2, μ(Mo-Kα) = 0.195 mm^{-1}, D_c = 1.192 g cm^{-3}, T = 120 K, 3575 measured and 3359 independent reflections, 224 parameters, R_1 ($I > 2\sigma(I)$) = 0.0321, wR_2 (all data) = 0.0880, GOF = 1.041. (*E*)-**4e**: $C_{14}H_{12}F_6N_2Si_2$, MW = 378.44, monoclinic, $P2_1/c$, a = 7.992(5) Å, b = 12.925(8) Å, c = 7.595(5) Å, β = 92.626(7)°, V = 783.7(8) Å^3, Z = 2, μ(Mo-Kα) = 0.290 mm^{-1}, D_c = 1.604 g cm^{-3}, T = 120 K, 1706 measured and 1339 independent reflections, 110 parameters, R_1 ($I > 2\sigma(I)$) = 0.0781, wR_2 (all data) = 0.2319, GOF = 1.096. Crystal data are available from the Cambridge Crystallographic Database Centre, deposition nos. CCDC 1057523 ((*E*)-**4a**), 1057524 ((*E*)-**4d**), 1057525 ((*E*)-**4e**) and 1057526 ((*Z*)-**4d**).

Density functional theory calculations.

Geometries of compounds (*E*)-**4e**, (*E*)-**5**, and (*E*)-**6** were fully optimized with density functional theory at the B3PW91/6-31G(d,p)[23] level using the Gaussian 09, Revision B.01 program.[24] Cartesian coordinates in optimized geometry of (*E*)-**4e**, (*E*)-**5**, and (*E*)-**6** are provided in Electronic Supplementary Information. The Kohn-Sham orbitals and vertical excitation energies were calculated at the B3PW91/6-311G++(2d,p) level.

Conclusions

The conclusions section should come in this section at the end of the article, before the acknowledgements. In this paper, we described the synthesis of some (*E*)-4,4′-dimethyl-2,2′-disilylazobenzenes. Their structures were confirmed both in the crystalline and solution states. The existence of at least one fluorine atom on each silicon atom is crucial to form the double intramolecular N···Si coordination. They showed bathochromic shifts of the π,π* transitions in the absorption spectra from that of non-substituted azobenzene. While most azobenzenes do not fluoresce at all, (*E*)-4,4′-dimethyl-2,2′-disilylazobenzene (*E*)-**4e**, which isomerizes reversibly to the (*Z*)-isomer, fluoresced a yellow-green colour at room temperature. The photoisomerizability accompanying the fluorescence emission property is remarkably different from hitherto known azobenzene derivatives. The fluorescence emission of (*E*)-**4e** is explained by the radiative relaxation because of the allowed π,π* transition from the lowest singlet excited state as a result of the inverted order of the n,π* and π,π* transitions of the azobenzene moiety because of the double N···Si coordination. The N···Si coordination is strong enough to cause a perturbation of the electronic structure, but weak enough to be cleaved upon photoexcitation. The moderate strength of the double N···Si coordination should be important for realization of both the photoisomerization and fluorescence emission properties of the azobenzene moiety. After the photoisomerization of (*E*)-**4e** to the corresponding (*Z*)-isomer, their mixture hardly fluoresces. Such a drastic change in the fluorescence intensity upon photoisomerization will be useful for regulation of the fluorescence property, and it is a unique photoisomerizable fluorophore to regulate the fluorescence intensity using a single light source.

Acknowledgements

The authors acknowledge financial supports of the Grants-in-Aid for Scientific Research on Innovative Areas “Coordination Programming” (No.22108508) and for Young Scientists (A) (No. 22685005) from the Ministry of Education, Culture, Sports, Science and Technology, Japan.

Notes and references

1 (a) S. Muramatsu, K. Kinbara, H. Taguchi, N. Ishii and T. Aida, *J. Am. Chem. Soc.*, 2006, **128**, 3764. (b) G. Pace, V. Ferri, C. Grave, M. Elbing, C. von Hänisch, M. Zharnikov, M. Mayor, M. A. Rampi and P. Samorı, *Proc. Natl. Acad. Sci. USA*, 2007, **104**, 9937. (c) A. A. Beharry and G. A. Woolley, *Chem. Soc. Rev.*, 2011, **40**, 4422. (d) E. Merino and M. Ribagorda, *Beilstein J. Org. Chem.*, 2012, **8**, 1071.
2 (a) N. Tamai and H. Miyasaka, *Chem. Rev.*, 2000, **100**, 1875. (b) A. Cembran, F. Bernardi, M. Garavelli, L. Gagliardi and G. Orlandi, *J. Am. Chem. Soc.*, 2004, **126**, 3234. (c) H. M. Dhammika Bandara, T. R. Friss, M. M. Enriquez, W. Isley, C. Incarvito, H. A. Frank, J. Gascon, and S. C. Burdette, *J. Org. Chem.*, 2010, **75**, 4817. (d) H. M. D. Bandara and S. C. Burdette, *Chem. Soc. Rev.*, 2012, **41**, 1809. (e) M. Quick, A. L. Dobryakov, M. Gerecke, C. Richter, F. Berndt, I. N. Ioffe, A. A. Granovsky, R. Mahrwald, N. P. Ernsting and S. A. Kovalenko, *J. Phys. Chem. B*, 2014, **118**, 8756.
3 H. Rau, in *Photochromism: Molecules and Systems*, ed. H. Durr and H. Bouas-Lauran, Elsevier, Amsterdam, 1990, p. 165.
4 M. Nepras, S. Lunák, Jr., R. Hrdina, J. Fabian, *Chem. Phys. Lett.*, 1989, **159**, 366.
5 (a) Y. Wakatsuki, H. Yamazaki, P. A. Grutsch, M. Santhanam and C. Kutal, *J. Am. Chem. Soc.*, 1985, **107**, 8153. (b) M. Ghedini, D. Pucci, G. Calogero and F. Barigelletti, *Chem. Phys. Lett.*, 1997, **267**, 341. (c) M. Ghedini, D. Pucci, A. Crispini, I. Aiello, F. Barigelletti, A. Gessi and O. Francescangeli, *Appl. Organomet. Chem.*, 1999, **13**, 565. (d) I. Aiello, M. Ghedini and M. La Deda, *J. Lumin.*, 2002, **96**, 249.
6 J. Azuma, A. Shishido, T. Ikeda, N. Tamai, *Mol. Cryst. Liq. Cryst.*, 1998, **34**, 83.
7 (a) M. Han and M. Hara, *J. Am. Chem. Soc.*, 2005, **127**, 10951. (b) M. R. Han and M. Hara, *New J. Chem.*, 2006, **30**, 223. (c) X. Ran, H. Wang, L. Shi, J. Lou, B. Liu, M. Li and L. Guo, *J. Mater. Chem. C*, 2014, **2**, 9866.
8 F. M. Raymo and M. Tomasulo, *J. Phys. Chem. A*, 2005, **109**, 7343.
9 (a) M. Shimomura and T. Kunitake, *J. Am. Chem. Soc.*, 1987, **109**, 5175. (b) A. Jacquart, R. M. Williams, A. M. Brouwer and E. Ishow, *Chem. Eur. J.*, 2012, **18**, 3706.
10 S. Tsuchiya, *J. Am. Chem. Soc.*, 1998, **121**, 48.
11 (a) J. Yoshino, N. Kano and T. Kawashima, *Chem. Commun.*, **2007**, 559. (b) J. Yoshino, N. Kano and T. Kawashima, *Chem.*

Lett., 2008, **37**, 960. (c) J. Yoshino, A. Furuta, T. Kambe, H. Itoi, N. Kano, T. Kawashima, Y. Ito and M. Asashima, *Chem. Eur. J.*, 2010, **16**, 5026. (d) H. Itoi, T. Kambe, N. Kano and T. Kawashima, *Inorg. Chim. Acta*, 2012, **381**, 117. (e) J. Yoshino, N. Kano and T. Kawashima, *Dalton Trans.*, 2013, **42**, 15826.

12 N. Kano, A. Furuta, T. Kambe, J. Yoshino, Y. Shibata, T. Kawashima, N. Mizorogi and S. Nagase, *Eur. J. Inorg. Chem.*, **2012**, 1584.

13 (a) N. Kano, F. Komatsu and T. Kawashima, *J. Am. Chem. Soc.,* 2001, **123**, 10778. (b) N. Kano, M. Yamamura, F. Komatsu and T. Kawashima, *J. Organomet. Chem.,* 2003, **686**, 192. (c) N. Kano, M. Yamamura and T. Kawashima, *J. Am. Chem. Soc.,* 2004, **126**, 6250. (d) N. Kano, F. Komatsu, M. Yamamura and T. Kawashima, *J. Am. Chem. Soc.,* 2006, **128**, 7097. (e) M. Yamamura, N. Kano and T. Kawashima, *Tetrahedron Lett.,* 2007, **48**, 4033. (f) M. Yamamura, N. Kano and T. Kawashima, *J. Organomet. Chem.,* 2007, **692**, 313.

14 (a) Y. Tokoro, H. Yeo, K. Tanaka and Y. Chujo, *Chem. Commun.*, 2012, **48**, 8541. (b) Q. Xiao, X. Meng, M. Kanai and Y. Kuninobu, *Angew. Chem. Int. Ed.*, 2014, **53**, 3168. (c) T. Wakaki, M. Kanai and Y. Kuninobu, *Org. Lett.*, 2015, **17**, 1758.

15 M. Yamamura, N. Kano, T. Kawashima, T. Matsumoto, J. Harada and K. Ogawa, *J. Org. Chem.*, 2008, **73**, 8244.

16 Crystal structures of (*E*)-**4a** is also determined. See, Supporting Information.

17 A. Bondi, *J. Phys. Chem.,* 1964, **68**, 441.

18 (a) C. Brelière, F. Carré, R. J. P. Corriu, M. Poirier and G. Royo, *Organometallics*, 1986, **5**, 388. (b) E. A. Williams and J. D. Cargioli, in *Annual Reports on NMR Spectroscopy*, ed. G. A. Webb, Academic Press, New York, 1979, vol. 9, p. 221.

19 S. Yamamoto, N. Nishimura and S. Hasegawa, *Bull. Chem. Soc. Jpn.* **1971**, *44*, 2018.

20 T. Fujino, S. Yu. Arzhantsev and T. Tahara, *J. Phys. Chem. A*, 2001, **105**, 8123.

21 J. Harada, K. Ogawa and S. Tomoda, *Acta Cryst.,* 1997, **B53**, 662.

22 (a) S. Yamaguchi and K. Tamao, *Bull. Chem. Soc. Jpn.*, 1996, **69**, 2327. (b) S. Yamaguchi and K. Tamao, *J. Chem. Soc., Dalton Trans.*, 1998, 3693.

23 J. P. Perdew, J. A. Chevary, S. H. Vosko, K. A. Jackson, M. R. Pederson, D. J. Singh, and C. Fiolhais, *Phys. Rev. B*, 1992, **46**, 6671.

24 Gaussian 09, Revision B.01, M. J. Frisch, G. W. Trucks, H. B. Schlegel, G. E. Scuseria, M. A. Robb, J. R. Cheeseman, G. Scalmani, V. Barone, B. Mennucci, G. A. Petersson, H. Nakatsuji, M. Caricato, X. Li, H. P. Hratchian, A. F. Izmaylov, J. Bloino, G. Zheng, J. L. Sonnenberg, M. Hada, M. Ehara, K. Toyota, R. Fukuda, J. Hasegawa, M. Ishida, T. Nakajima, Y. Honda, O. Kitao, H. Nakai, T. Vreven, J. A. Montgomery, Jr., J. E. Peralta, F. Ogliaro, M. Bearpark, J. J. Heyd, E. Brothers, K. N. Kudin, V. N. Staroverov, T. Keith, R. Kobayashi, J. Normand, K. Raghavachari, A. Rendell, J. C. Burant, S. S. Iyengar, J. Tomasi, M. Cossi, N. Rega, J. M. Millam, M. Klene, J. E. Knox, J. B. Cross, V. Bakken, C. Adamo, J. Jaramillo, R. Gomperts, R. E. Stratmann, O. Yazyev, A. J. Austin, R. Cammi, C. Pomelli, J. W. Ochterski, R. L. Martin, K. Morokuma, V. G. Zakrzewski, G. A. Voth, P. Salvador, J. J. Dannenberg, S. Dapprich, A. D. Daniels, O. Farkas, J. B. Foresman, J. V. Ortiz, J. Cioslowski and D. J. Fox, Gaussian, Inc., Wallingford CT, 2010.

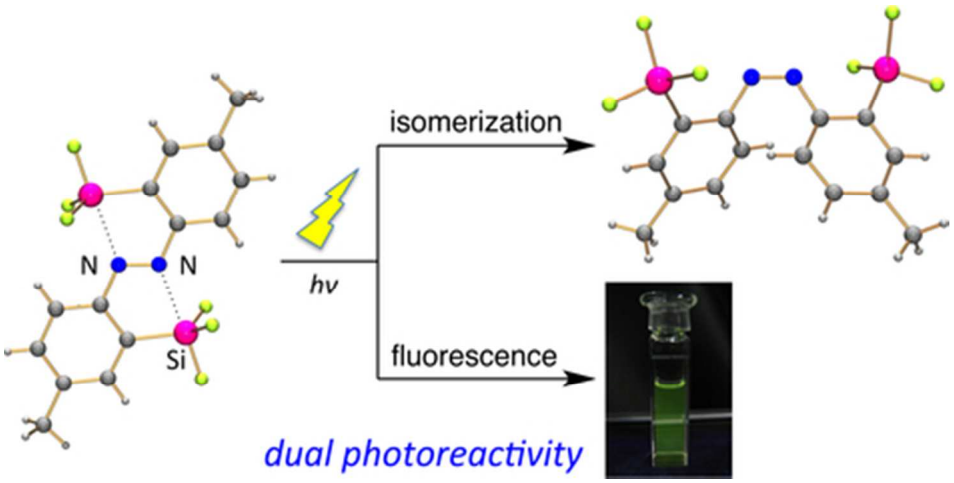

39x19mm (300 x 300 DPI)